ARTICLE

Check for updates

Subaerial volcanism is a potentially major contributor to oceanic iron and manganese cycles

Jack Longman [1,2✉], Martin R. Palmer[2], Thomas M. Gernon [2], Hayley R. Manners [2,3] & Morgan T. Jones [4]

Surface ocean availability of the micronutrients iron and manganese influences primary productivity and carbon cycling in the ocean. Volcanic ash is rich in iron and manganese, but the global supply of these nutrients to the oceans via ash deposition is poorly constrained. Here, we use marine sediment-hosted ash composition data from ten volcanic regions, and subaerial volcanic eruption volumes, to estimate global ash-driven nutrient fluxes. Using Monte Carlo simulations, we estimate average fluxes of dissolved Iron and Manganese from volcanic sources to be between 50 and 500 (median 180) and 0.6 and 3.2 (median 1.3) Gmol yr^{-1}, respectively. Much of the element release occurs during early diagenesis, indicating ash-rich shelf sediments are likely important suppliers of aqueous iron and manganese. Estimated ash-driven fluxes are of similar magnitude to aeolian inputs. We suggest that subaerial volcanism is an important, but underappreciated, source of these micronutrients to the global ocean.

[1] Marine Isotope Geochemistry, Institute for Chemistry and Biology of the Marine Environment (ICBM), University of Oldenburg, Carl von Ossietzky Straße 9-11, 26129 Oldenburg, Germany. [2] School of Ocean and Earth Sciences, University of Southampton, Southampton SO14 3ZH, UK. [3] School of Geography, Earth and Environmental Sciences, University of Plymouth, Plymouth PL4 8AA, UK. [4] Centre for Earth Evolution and Dynamics (CEED), Department of Geosciences, University of Oslo, Sem Sælands vei 2A, 0371 Oslo, Norway. ✉email: jack.longman@uni-oldenburg.de

Primary production in the oceans is a major driver of the biogeochemical carbon cycle[1,2], largely controlling carbon dioxide (CO_2) exchange between oceanic and atmospheric carbon pools. The drawdown of atmospheric CO_2 via photosynthetic phytoplankton represents one of the largest atmospheric carbon sinks in the Earth System today, removing ~50 gigatons (Gt) carbon per year[3]. The importance of micronutrients, and in particular iron (Fe), in controlling levels of primary production has long been recognised[4,5], with Fe essential to many biological processes[4]. Manganese (Mn) is also essential for phytoplankton photosynthesis[6], with evidence it may act as a co-limiting nutrient[7], especially in parts of the ocean containing low levels of dissolved Fe[8].

There are multiple ways through which volcanoes may affect the climate on a range of timescales from hours to millions of years[9,10]. Volcanism can induce global climatic cooling via radiative forcing from sulfate injection[11], but also potentially by oceanic fertilisation associated with the input of nutrient-rich ash[12–15]. Although experimental evidence demonstrates the release of nutrients from freshly-deposited ash (defined as all airborne volcanic particles under 2 mm in diameter) in surface seawater[16], the impacts of this process appear to be restricted to transient algal blooms observed directly after eruptions[17,18]. In these cases, discrete eruptions may briefly alleviate nutrient deficiencies by providing a source of dissolved Fe[10,17,19]. Manganese supply from ash may also contribute to increases in productivity, with the addition of both Fe and Mn appearing to relieve Mn co-limitation after ash deposition[20].

The major well-established routes by which dissolved Fe and Mn are delivered to the oceans are dissolved fluvial outflow, hydrothermal venting and desert dust deposition[4,21,22]. Although ash deposition has been invoked as a source of nutrients locally[16,22], it is not generally considered in models of oceanic trace metal cycling[21,23]. Olgun et al.[19] compiled volcanic eruption rate data and undertook experimental studies of the amount of dissolved Fe released (over the course of 60 mins) by different types of fresh volcanic ash. This study concluded that $128–221 \times 10^{12}$ g yr^{-1} of ash is delivered to the Pacific Ocean, releasing 0.003–0.075 Gmol yr^{-1} of dissolved Fe to surface waters. This flux is comparable to the flux of dissolved Fe delivered to the Pacific Ocean by non-volcanic mineral dust (0.001–0.065 G mol yr^{-1})[24].

Given the potential importance of volcanism for oceanic nutrient availability, we have sought to constrain the magnitude of the global dissolved Fe flux from a different perspective. We compare the composition of fresh ash from 10 active volcanic regions globally (Fig. 1) with the composition of ash recovered from marine sediments of various ages (Supplementary Fig. 1), to estimate the loss of Fe and Mn over a longer timescale than permitted in experimental studies (cf. ref. [19]). We combine this approach with the most recently available constraints on global volcanism rates derived from the Global Volcanism Program[25] to provide estimates of global volcanogenic Fe and Mn supply. The longer timescale approach is analogous to studies of dissolved and colloidal Fe released from shelf sediments during long-term diagenesis, which is known to be an important source of Fe to surface waters where it can stimulate phytoplankton growth[26].

Results and discussion

Diagenetic release of Fe and Mn from ash. Depletion factors, representing the difference between unaltered and altered ash metal contents (see Methods), for Fe (median 45% depletion) and Mn (median 20% depletion) suggest that a large proportion of these elements in ash is available to be released into seawater during particle settling and early diagenesis (Fig. 2). These Fe depletion factors are higher than those observed under laboratory

conditions[19]. This is likely because Fe and Mn release continues much longer than the duration of such experiments, as a consequence of diagenetic processes once ash settles to the seafloor[14,27].

While experimental work suggests that basaltic ash releases higher absolute Fe concentrations during dissolution than silicic ash[28], the results from our study suggest that the rhyolitic ashes from the Taupo and Aleutian arcs proportionally (and counterintuitively) release the most Fe and Mn (Fig. 2). This unexpected relationship may be due to a higher ratio of surface-bound Fe to intra-silicate Fe in these samples[29], and may not be indicative of greater absolute Fe and Mn release. Alternatively, this discrepancy may be linked to variations in secondary clay precipitation, a process which is controlled by a range of mineralogical and compositional factors, resulting in differing rates of ash alteration[30].

Another factor that likely determines the rates of Fe and Mn release and depletion factor differences is grain size variations. Basaltic ash generally contains fewer very fine (<30 to 60 µm) particles (<1–4%) than rhyolitic and silicic ash (30 – >50%) due to their eruption characteristics[31]. Thus, rhyolitic ashes (such as those from the Taupo arc) likely contain a greater proportion of fine particles, with a greater surface area/volume ratio, that react more extensively with seawater[10].

Ashes from the Central American Volcanic Arc (Fig. 1a) show a distinctive behaviour from the other sites, with a large range of Fe depletion factors, and a number of ash layers demonstrating net adsorption of Fe (Fig. 2). The uptake of Fe and Mn by the ash may arise from the high nutrient supply in this area, as a result of equatorial upwelling of nutrient-rich Southern Ocean waters[32–34]. Pore water measurements from the region show that Mn (and Fe) are concentrated in the uppermost sedimentary layers, a result of the diffusive flux of these elements from deeper, suboxic sediment[35].

Global annual flux of Fe and Mn from ash diagenesis. The overall trends of depletion of Fe and Mn in ash recovered from marine sediments indicate that ash may be an important source of these nutrients to oceanic environments. Using a Monte Carlo modelling approach, we probabilistically estimated the most likely values for global annual input of Fe and Mn to the oceans arising from this process (see Methods). We employed well-constrained ranges of variables, which include annual ash production rates; ash geochemistry; ash density; and ash dispersal, to estimate overall Fe and Mn supply rates. The main aim of this exercise is to determine the net fluxes of dissolved Fe and Mn arising from the alteration of ash, rather than to study the specific geochemical and mineralogical processes that control these fluxes.

As we consider estimates of numerous variables in the construction of our model, each characterised by their own error, the use of a probabilistic approach is considered the most suitable. For example, the depletion factor values developed here are considered to represent the full range of feasible volcanic ash compositions, and thus, the mean and standard deviation of the dataset represent a credible range of values. As such, this variable is likely well-constrained. However, variables such as the amount of ash entering the ocean from each volcanic province (see Methods), which despite being based on a method developed that considers prevailing winds and the weathering and post-depositional transport (via waterways and re-suspended material) of subaerially deposited ash[19,36], is still uncertain. To tackle this problem, we apply additional error estimates to those values resulting in higher standard deviations, which help represent the inherent uncertainty of these variables.

Models of the biogeochemical Fe cycle typically consider four main sources of dissolved Fe; atmospheric deposition (comprising dust, fire and industrial sources), dissolved fluvial input, marine sediment diagenesis, and hydrothermal venting[22,37] (Table 1). Our simulations
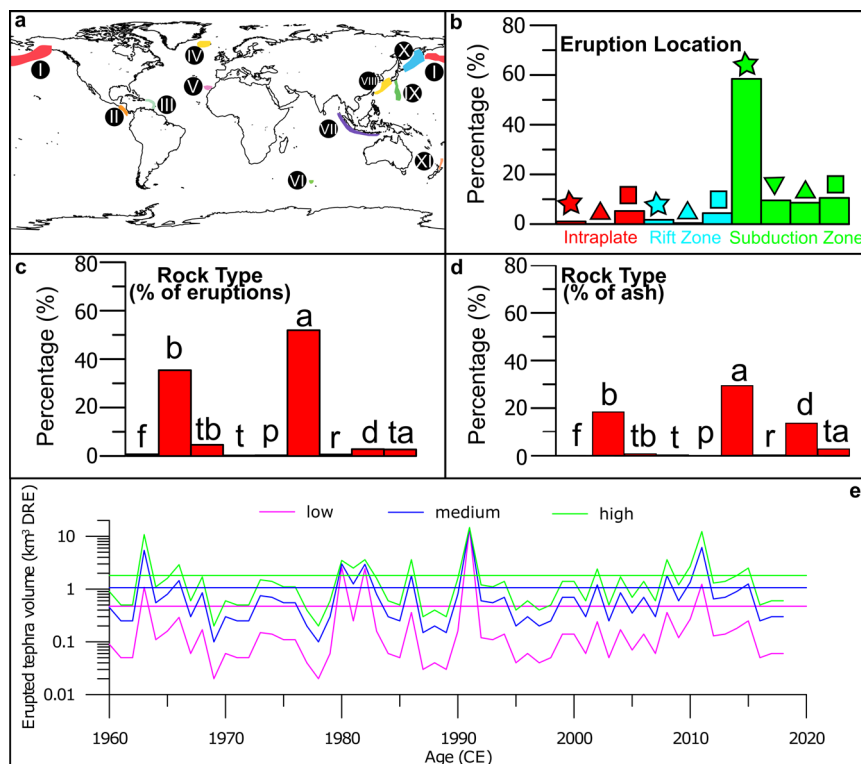
Fig. 1 Global map indicating volcanic provinces used in this study, and compilation of data from the Global Volcanism Program (GVP). a Source regions used to construct unaltered protolith compositions, indicated by numbers and coloured shading: (I) Aleutian Island arc, (II) Central American volcanic arc, (III) Lesser Antilles island arc, (IV) Iceland, (V) Azores, (VI) Kerguelen, (VII) Sunda arc, (VIII) Kyushu-Ryukyu arc, (IX) Izu-Bonin arc, (X) Kamchatka-Kurile arc, (XI) Taupo volcanic zone. Map was created using the vector shorelines of ref. [66]. **b** Percentage of eruption events occurring at each type of volcanic location, denoted by colour and symbols for fully continental (star), intermediate locations on plate boundaries (upward-pointing triangle), oceanic (square) and unknown (downward-pointing triangle). **c** Proportion of each rock type as a percentage of all eruptive events since 1960. Rock types are foidite (f), basalt (b), trachybasalt (tb), trachyte (t), phonolite (p), andesite (a), rhyolite (r), dacite (d) and trachyandesite (ta). **d** Proportion of each rock type as a percentage of all ash deposited via eruptions since 1960, with rock types labelled as in panel **c**. **e** Erupted ash volume (in km^3 DRE) of each year since 1960, using GVP data representing the three ash volume scenarios (see Methods); 'low' (pink line), 'medium' (blue line) and 'high' (green line). The horizontal lines indicate the average values for each of the scenarios; 0.47 $km^3 \, yr^{-1}$ for 'low', 1.07 $km^3 \, yr^{-1}$ for 'medium and 1.81 $km^3 \, yr^{-1}$ for 'high'.

suggest a net flux of between 90–500 Gmol Fe yr^{-1} (representing median values of the 'small' and 'large' ash volume scenarios; see Methods) to the oceans from ash deposition, dissolution, and diagenesis (Fig. 3). The median value derived from the 'medium' ash scenario (180 Gmol Fe yr^{-1}) is higher than estimates of global dissolved fluvial Fe flux (27 Gmol Fe yr^{-1}) and greater than the authigenic Fe flux (90 Gmol Fe yr^{-1}) and that related to coastal erosion (140 Gmol Fe yr^{-1}; refs. [5,38]). They are on the same order as postulated dust inputs, but this value does not consider the solubility of Fe in dust, estimated to be <1–4% (refs. [22,39]). Hence, the available Fe from dust sources (calculated as 3–11 Gmol Fe yr^{-1}) is likely lower than our estimates of ash diagenesis input.

We now consider Mn fluxes related to this process. In current models of the Mn biogeochemical cycle, oceanic inputs are thought to derive predominantly from dissolved fluvial inputs (0.3 Gmol Mn yr^{-1}), dust (5.6 Gmol Mn yr^{-1}) and hydrothermal activity (102 Gmol Mn yr^{-1}; ref. [21]). Our simulations suggest a likely net flux from ash diagenesis of 0.6–3.2 Gmol Mn yr^{-1}, (Fig. 3), with the median value from the 'medium' scenario of 1.3 Gmol Mn yr^{-1} comparable with both dissolved fluvial flux and atmospheric deposition, but smaller than the hydrothermal Mn flux (Table 1) and particulate fluvial flux[40].

Implications for modern Fe and Mn cycles and the carbon cycle. Our estimates of the Fe (and to a lesser extent Mn) supply to the oceans from ash diagenesis are of the same order of magnitude as other sources (e.g., atmospheric deposition and

dissolved riverine flux) and highlights the need to include this process in global budgets[19]. However, while most other Fe sources are not expected to show rapid changes in magnitudes over geologically short intervals, explosive subaerial volcanic activity can show large (and apparently stochastic) variations over short time intervals. For example, while the global annual average eruption rate of ash is ~1 km^3 ash dense rock equivalent (DRE), the eruption of Mount Pinatubo in 1991 (Volcanic Explosivity Index (VEI) 6) released more than 5 km^3 of ash within a matter of days. Much of this ash was rapidly deposited in the ocean, covering roughly $4 \times 10^6 \, km^2$ of the South China Sea[41].

Furthermore, the nature of ash supply to the oceans may mean that a large proportion of the nutrients are released in the upper ocean. Firstly, most volcanoes are located close to the oceans (Fig. 1), and ash will be supplied directly to the upper ocean and may be directly bioavailable. To provide an approximate estimate of bioavailability, we use the experimental data of ref. [36], wherein ash from Montserrat (Caribbean Sea) was exposed to seawater to simulate dissolution for 6 months. We calculate that during this period, ~0.4% of the total Fe, and ~14% of the total Mn originally hosted in the ash was released (Supplementary Fig. 2), but that the reaction was still ongoing. These proportions appear small but when scaled up using our models, correspond to between 0.82 and 4.43 Gmol Fe yr^{-1}, on the same order of magnitude as aeolian dust supply[5] (Table 1). For Mn, the loss of 14% of the original ash content corresponds to between 0.18–0.99 Gmol Mn yr^{-1} being released in the upper ocean. The value of 14% Mn loss in the early
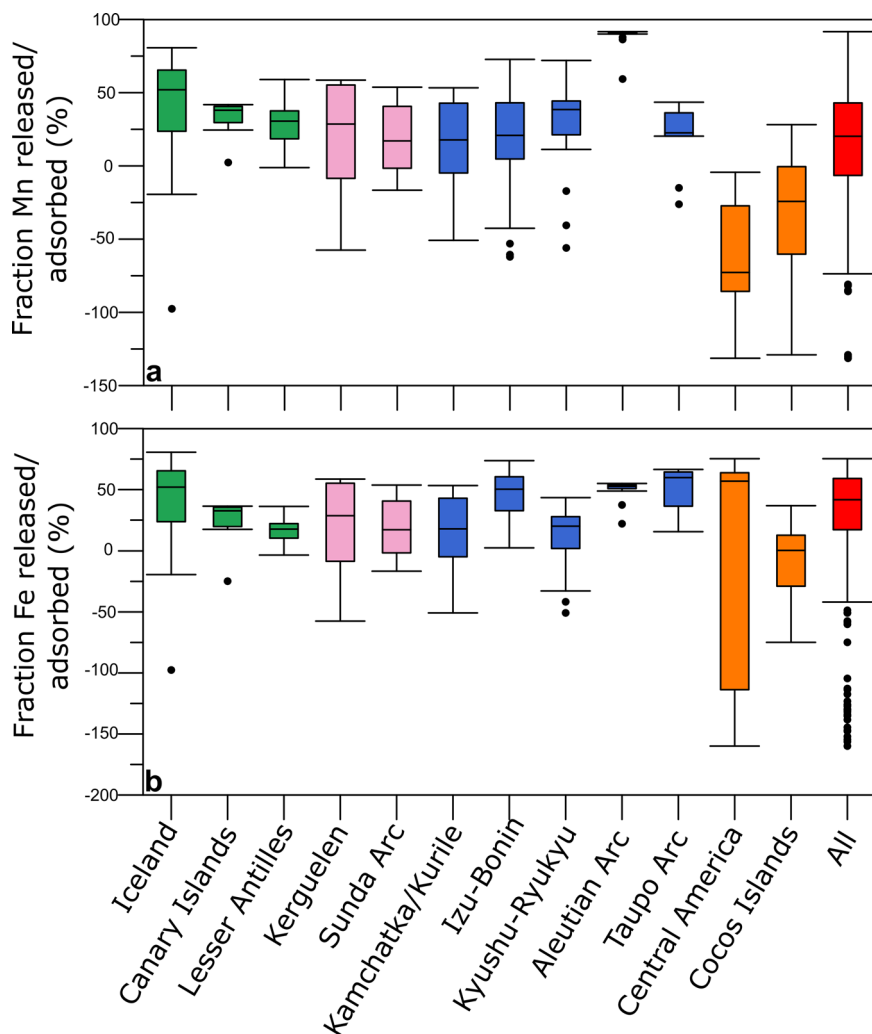
Fig. 2 Depletion factors for each volcanic province for both manganese and iron. Box plots detailing the distribution of depletion factor data from each volcanic province are presented for manganese (**a**) and iron (**b**), indicating likely levels of depletion/adsorption in each locality. Colour of the boxes indicates the ocean region of each province, either Atlantic (green), Indian (pink), North and West Pacific (blue) or East Pacific (orange). Boxes are defined between the first and third quartile (the interquartile range, IQR), with minimum and maximum whiskers representative of 1.5 times the IQR, and suspected outliers (>1.5 times the IQR) indicated by black circles.

stages of transport and burial represents 65% of total Mn depletion and suggests the bulk of Mn release occurs in this period (Supplementary Figs. 2 and 3).

Most of the ash deposited in the oceans settles on continental shelves (Fig. 1, ref. [42]), which represent an important source of Fe to the ocean system[43]. Once sediment is deposited on the shallow seafloor, diagenetic processes (e.g., biological action and redox reactions) and wave action result in the flux of soluble and colloidal fractions of Fe^{2+} (and Mn^{2+}) to the overlying water column[44]. These Fe- and Mn-enriched waters may then be advected into the open ocean[26], as evidenced by the positive relationship between dissolved Fe concentrations of ocean water and proximity to continental shelves[45]. As a large proportion of Fe release likely occurs during early diagenesis on continental shelves, volcanic ash dissolution may be a component of boundary exchange of dissolved Fe, a mechanism for transporting shelf-hosted nutrients out to the open ocean[46,47]. This is supported by studies showing high Fe content in some water masses affected by high volcanogenic sediment supply[48–50]. Analysis of the Fe isotopic composition of one such location, offshore of the Crozet Islands, indicates a volcanic signature of the dissolved Fe, related to volcanogenic sediment diagenesis and

weathering[51,52]. This is supported by Fe isotope evidence from the western Pacific Ocean[53,54] and the Southern Ocean[55], where isotopically heavy Fe is linked to non-reductive dissolution of shelf-sediment Fe-bearing phases. In view of this evidence, it appears that much of the Fe (and some of the Mn) added to the oceans via ash deposition may have previously been included in estimates of the overall sedimentary fluxes, rather than representing an entirely new flux (Table 1). Estimates of the magnitude of Fe release during diagenesis of shelf sediments vary widely. For example, in a recent sedimentary flux model comparison, estimates of Fe supply varied between 0.6 and 194 $Gmol\,yr^{-1}$ (ref. [23]). This highlights the need for further investigation into benthic fluxes on a shelf-by shelf basis, to provide quantitative estimates of Fe supply via weathering, followed by assessments of exactly how much of this flux is ash-related. Our work also indicates the need for models of biogeochemical cycling to consider the input of large, apparently stochastic events such as volcanic eruptions on Fe and Mn cycles. Such work may help indicate the impact of individual events, which supply a large amount of nutrients to certain area of the oceans, and how internal marine processes may act to cycle these inputs.

Table 1 Global Fe and Mn fluxes comparing previously published estimates of sources and the new estimates presented here.

	Annual Fe Flux (Gmol yr^{-1})
Fluvial particulate total iron[a]	11,192–17,226
Fluvial dissolved iron[a]	27
Glacial sediments[a]	609
Atmospheric (i.e., aeolian)[a]	287
Hydrothermal[a]	251
Authigenic[a]	90
Early release from ash[b]	0.8–4.4
Diagenetic release from ash[c]	91–493
Dust[d]	5.6
Fluvial dissolved Mn[d]	0.3
Sediment[d]	3.4
Hydrothermal[d]	102.3
Early release from ash[b]	0.18–0.99
Diagenetic release from ash[c]	0.39–2.19

[a]Estimates of Fe flux from ref. [5].
[b]Value of diagenetic Fe and Mn fluxes developed using our new estimates of global ash production and oceanic deposition and estimates of element release during 6-month experiment from ref. [65].
[c]Estimates of diagenetic Fe and Mn flux from this study, with the range representing the 'small' and 'large' ash deposition scenarios (see Methods and Supplementary Table 13).
[d]Estimates of Mn flux from ref. [21].

Methods

Major and trace element geochemistry. We analysed ash layers from IODP Holes U1396C (Lesser Antilles) and U1339D (Aleutian Islands). Ash layers were identified visually (at macro- and microscopic scales) in the case of Hole U1339D, and via their relatively low $CaCO_3$ contents in Hole U1396C. To avoid inclusion of pelagic sediment, only samples located within the centre of ash layers were used. Such an approach also circumvents the potential impact of bioturbation. Bulk sample geochemistry for Holes U1396C and U1339D was determined via a closed vessel Aqua Regia digest (at 60 °C), after which samples were dried, then further digested using a HF/HClO$_4$ mix (at 130 °C), followed by a HClO$_4$ digest (at 130 °C) before a final HCl dissolution. Digests were re-suspended in 2% HNO$_3$ and analysed on a Thermo Scientific X-Series inductively coupled plasma mass spectrometry (ICP-MS) at the University of Southampton. Alongside samples, blanks and a reference material (HISS-1 marine sediment standard) were prepared and analysed using the same procedure (Supplementary Table 1). Data from Hole U1396C were supplemented by previously published values[56].

Chemical depletion factors. In addition to newly analysed ash layers from the Lesser Antilles and the Aleutian Islands, a database of previously published altered marine ash compositions was compiled from a selection of volcanic settings, from subduction zones (e.g., Aleutian Arc, Kamchatka), convergent margins (e.g., Taupo Volcanic Zone, Izu-Bonin Arc) and oceanic islands (e.g., Canary Islands) (Fig. 1 and Supplementary Table 2). Most of these data come from point-based geochemical methods (electron microprobe and laser ablation ICP-MS) of individual ash shards.

Unaltered protolith compositions were obtained from the GeoRoc database (http://georoc.mpch-mainz.gwdg.de) for volcanic material from the source regions for each of the published marine ash compositions. These data were filtered to remove data relating to non-outcropping subaerial samples, xenoliths, and any inclusion-based analyses, leaving only measurements of bulk igneous rock compositions. The database was used to reconstruct the most likely original composition of the erupted material prior to marine diagenesis. The comparison of bulk rock compositions to point-based glass shard analyses may result in an overestimation of depletion. This is because the glass in mafic ash will contain low Fe, but the accompanying minerals (for example pyroxenes) may have a high Fe content, but will not be considered in the measurements, leading to anomalously high depletion factors. However, glass typically makes up the majority of volcanic ash, and even in Fe rich minerals, Fe would not comprise the entirety of the material, so we believe our comparison is valid.

The method follows that developed by ref. [12] to calculate metal mobility in Cretaceous ash layers, in which the elements of interest (M) are normalised to the Ti and Zr concentrations. These elements are largely immobile during diagenesis[57], so variations in their concentrations in ash derived from a single source largely reflect magmatic differentiation processes[12]. The empirical relationship between Ti/Zr and M/Zr (as calculated from the GeoRoc database) can then be used to estimate the original composition of the unaltered volcanic protolith (Fig. 4). In each case, the empirical relationship is represented by a linear or polynomial regression (Supplementary Table 2), and the equations are used to back-calculate
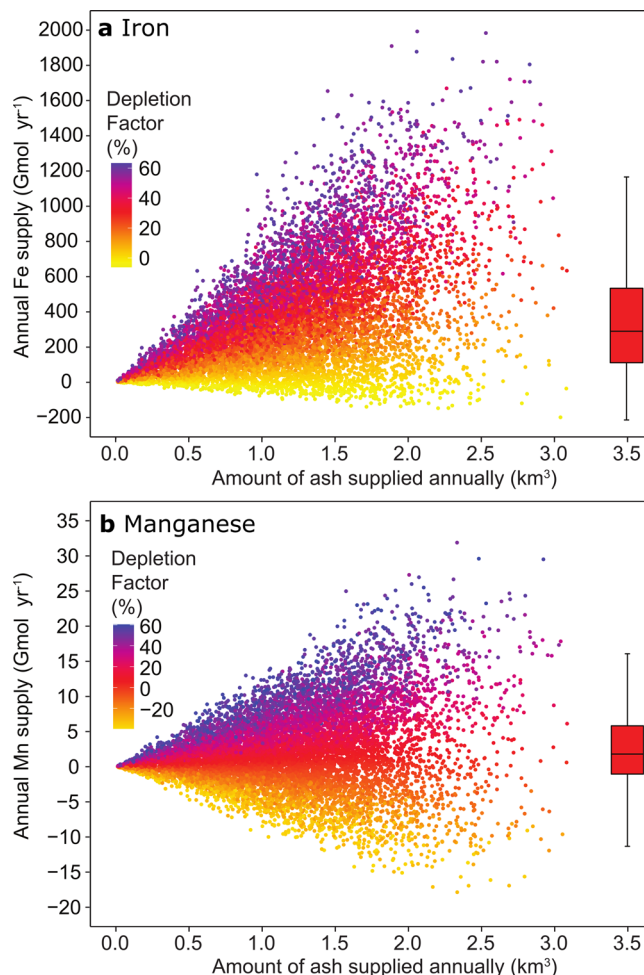
Fig. 3 Monte Carlo simulations of likely Iron and Manganese supply to the oceans annually, representative of the 'medium' ash volume scenario. Presented are simulations for iron (**a**) and manganese (**b**). For both panels the amount of ash supplied annually is presented along the x-axis, with the total annual supply of the element on the y-axis. These Monte Carlo simulations are indicated by circles, with their colour indicating the depletion factor used in the simulation. A summary of the data is presented as a box plot on the right of each panel, developed in the same manner as those shown in Fig. 2.

the unaltered protolith composition. The best fitting regression is determined by both examination of the correlation coefficient, but also by determination of which fit best suits the altered tephra dataset. For example, with Iceland we employ polynomial regression, due to the low Fe/Zr ratios of most tephra compositions. Here, a linear relationship would not represent these data well, and lead to underestimation of the depletion factor (Supplementary Fig. 4). These compositions are then compared to the marine ash data to calculate changes in composition during diagenesis[12] according to Eq. (1), which is shown here using Fe as the element of interest, as an example:

$$Fe_D = \frac{M_{Fe}^L}{M_{Fe}^O} = 1 - \frac{\left(\frac{C_{Fe}^{re}}{C_{Zr}^{re}}\right)}{\left(\frac{C_{Fe}^O}{C_{Zr}^O}\right)} \tag{1}$$

The left side of the equation represents the fraction depleted, where M_{Fe}^O is the original mass of Fe in the rock, and M_{Fe}^L what has been lost. C_{Fe}^{re} and C_{Zr}^{re} *are* the concentrations of Zr and Fe in the altered ash, and so C_{Fe}^{re}/C_{Zr}^{reO} represents the Fe/Zr ratio in the ash. C_{Fe}^O/C_{Zr}^O represents the Fe/Zr ratio in the original rock, calculated using the GeoRoc-derived relationship between Fe/Zr and Ti/Zr (e.g., Fig. 4). Graphs of M/Zr vs. Ti/Zr for all locations are provided in Supplementary Figs. 4–7.

To estimate annual inputs of Fe and Mn to the ocean from ash diagenesis, a Monte Carlo-based modelling approach (c.f. [58]) is applied using likely ranges of
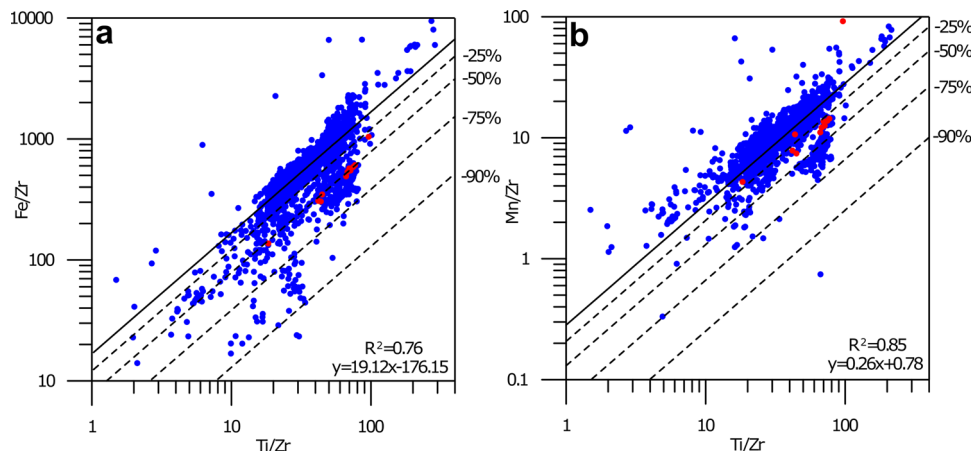
Fig. 4 Plots of Fe/Zr and Mn/Zr vs. Ti/Zr for the Aleutian arc. Presented here are data for (**a**) Fe and (**b**) Mn. In blue are GeoRoc-derived protolith compositions, from which the linear relationships indicated the lower right of each panels are defined. Red circles indicate measured altered ash deposit analyses, plotted against the expected trend for unaltered material. The dashed lines indicate the percentage depletion. Similar graphs for all other active volcanic regions can be found in Supplementary Figs. 4–7.

each of the pertinent parameters. For each variable, the r package *rtruncnorm* was used to generate 10,000 random data points between two boundaries assuming a normal distribution according to defined mean and standard deviation values (Table 1).

Annual ash fluxes to the ocean are estimated from data derived from the Global Volcanism Program database (GVP; ref. [25]). This database contains the location, style and intensity of volcanic activity (Supplementary Tables 3, 4, 5), and was used in association with GeoRoc to estimate the elemental composition of erupted ash (Fig. 1b, e). In our analysis, we limit the data from GVP to eruptions from the start of 1960 to the end of 2019, as before 1960 the knowledge of smaller eruptions becomes less certain. Using the GVP's archive of VEI (Supplementary Table 5), we estimated the amount of ash erupted annually, by converting the VEI of eruptions into dense rock equivalent (DRE) volume. Since small eruptions are unlikely to result in ash plumes and are insignificant in terms of ash delivery to the oceans, we do not consider any eruptions ≤VEI 2. As a VEI indicates a range of potential volumes (e.g., VEI 5 is 1–10 km³ DRE), for each eruption we produce three possible scenarios; a low (e.g., 1 km³ for VEI 5), medium (e.g., 5 km³ for VEI 5) and high (e.g., 10 km³ for VEI 5) scenario. Wherever possible, we constrain larger eruption estimates using published data (see Supplementary Table 6). We use our 'low', 'medium' and 'high' scenarios to attain three estimates of ash deposition for each year. We then sum and average the values of each scenario for each year, yielding three estimates of yearly ash input: a 'low' scenario of 0.47 km³ yr⁻¹, a 'medium' scenario of 1.07 km³ yr⁻¹ and a 'high' scenario of 1.81 km³ yr⁻¹ (Fig. 1e), all of which are broadly consistent with an earlier estimate of 1 km³ yr⁻¹ (ref. [59]). Using the average and standard deviation of each scenario, we run 10,000 simulations of ash volume per year, and use these values in our estimates of Fe and Mn supply, resulting in estimation of total Mn and Fe supply for three scenarios (Fig. 3 and Supplementary Fig. 8).

One limitation of using the period 1960–2019 is that we do not include any eruptions >VEI 6, since the last was Tambora in 1815. To assess the impact of such an event on our estimates, we calculate (using the same approach as above), the ash flux for all eruptions between VEI 2 and VEI 4 from 1960–2019, which yields a value of 0.57 km³ yr⁻¹ (Supplementary Fig. 9). Assuming this is representative of background ash flux (i.e., all eruptions smaller than VEI 5), we take this as a baseline value for flux back to 1800, and add in all larger eruptions, using published data for volumes wherever possible (Supplementary Fig. 9 and Supplementary Table 6). By averaging these data, we obtain an estimate of annual ash flux of 1.42 km³ yr⁻¹, greater than the estimate derived from the period 1960-Present (Supplementary Fig. 9). This indicates how these periodic large events may play a controlling role in total ash volumes and indicating that our first approach may yield an underestimation. However, the incompleteness of eruption data prior to 1960 means we do not use this value in modelling.

To account for the composition of erupted ash, we categorise all eruptions according to their eruption style (Supplementary Tables 3,4) and assess the percentage contribution of each style of eruption (Fig. 1b). Using lithological data available through GeoRoc, we estimate the Fe and Mn concentrations in material supplied from each volcanic source, and using the percentage of eruptions from the GVP, convert this to absolute ranges in composition (Supplementary Tables 7 and 8). This exercise suggests that, on average, ash (i.e., a combination of all ash types, locations and eruptions styles) contains 6 ± 1 wt.% Fe and 0.12 ± 0.02 wt.% Mn (Supplementary Table 9). To convert from volume to density we use an average ash density of 1400 kg/m³, with a standard deviation of 133 kg/m³ (ref. [60]). Finally, we use the depletion factors

derived above, to convert from absolute values of Fe and Mn to the amount released to the oceans during ash transport and diagenesis. For these values we use mean depletion factors, and the standard deviation of the entire dataset (Supplementary Table 10). To avoid unreasonable under- or overestimation, we place boundaries derived from the 10 and 90% percentiles of the data to our simulations (Supplementary Table 10).

To ensure we do not include ash which does not fall into the ocean, we sort the GVP data by sub-region, and estimate the proportion of ash, which falls into the ocean at each location (using prevailing wind directions and the position of the sub-region, cf. ref. [19]). In making these estimates, we directly consider published isopachs and examples of marine sedimentary deposition from each of the regions (see Supplementary Table 11). This approach relies upon several assumptions, namely that wind directions may not be in the prevailing direction when a volcano erupts. To account for this, we have included conservative estimates for ash fall, and large errors for those that are more uncertain (see Supplementary Table 11). For example, even for mid-ocean regions that are located on small islands (such as Vanuatu and Jan Mayen), we only estimate 85% of ash falling into the ocean, when it is likely to be higher. Further, by using Monte Carlo modelling, we incorporated the uncertainty in this value into the estimate. We use GVP data to investigate the number of each size of eruptive event from each region, deriving three scenarios ('low', 'medium' and 'high') of ash volume for each individual region in a similar manner to our estimate of total ash volume (Supplementary Table 12). From this we derive three estimates of ash volume for each of the regions. We use the results of the 'medium' scenario to inform further modelling. This is because it represents a middle point in possible ash volumes and is likely to be closest to the truth with respect to the magnitude of ash weathering. This process occurs when fresh ash is weathered via surface runoff, with the content of the ash leached, to then enter the ocean in particulate or dissolved forms[36,61]. Evidence for the scale of this process may come from Montserrat, where Fe and Mn levels in rivers, which drain fresh ash are enriched when compared to those which do not[36]. Further, large quantities of subaerially deposited ash may be re-suspended and transported to the oceans, as was observed across Iceland in the aftermath of the Eyjafjallajökull eruption in 2010[62], and pumice rafting may act to transport ash further away from eruption locations[63,64]. Using this method does not allow us to indicate exactly how fast the depletion occurs, but evidence suggests there is no link between ash age and depletion factor (Supplementary Fig. 1), indicating that depletion occurs at an early stage of deposition and diagenesis.

Using the outputs from each simulation, we calculate results using Eq. (2) for calculation of the amount of Fe release:

$$\text{Fe release (mole)} = \left(\frac{V_{Ash} \times \rho_{Ash} \times \text{Fe}_{Ash} \times \text{Fe}_D}{55.845} \right) \times P_{ocean} \quad (2)$$

where V_{Ash} and ρ_{Ash} are the volume and density of ash, respectively, Fe_{Ash} is the average proportion of Fe in igneous rock as defined above, and Fe_D is the depletion of Fe as calculate using Eq. (1), 55.845 is the atomic mass of Fe, used to convert from grams to moles, and P_{ocean} is the proportion of ash that settles into the ocean. As we use three scenarios for the ash volume estimation, we derive three ranges of total Fe and Mn supply, from which we extract the median to indicate a likely value for each scenario and set of models (Supplementary Table 13).

Data availability

References

1. Del Giorgio, P. A. & Duarte, C. M. Respiration in the open ocean. *Nature* **420**, 379–384 (2002).
2. Field, C. B., Behrenfeld, M. J., Randerson, J. T. & Falkowski, P. Primary production of the biosphere: Integrating terrestrial and oceanic components. *Science (80-.)* **281**, 237–240 (1998).
3. Ciais, P. et al. In *Climate Change The physical Science Basis. Contribution of Working Group I to the Fifth Assessment Report of the intergovernmental Panel on Climate Change* (eds. Stocker, T. F. et al.) 465–570 (Cambridge University Press, 2013).
4. Tagliabue, A. et al. The integral role of iron in ocean biogeochemistry. *Nature* **543**, 51–59 (2017).
5. Jickells, T. D. et al. Global iron connections between desert dust, ocean biogeochemistry, and climate. *Science (80-.)* **308**, 67–71 (2005).
6. Raven, J. A. Predictions of Mn and Fe use efficiencies of phototrophic growth as a function of light availability for growth and of C assimilation pathway. *New Phytol* **116**, 1–18 (1990).
7. Wu, M. et al. Manganese and iron deficiency in Southern Ocean Phaeocystis antarctica populations revealed through taxon-specific protein indicators. *Nat. Commun.* **10**, 3582 (2019).
8. Peers, G. & Price, N. M. A role for manganese in superoxide dismutases and growth of iron-deficient diatoms. *Limnol. Oceanogr.* **49**, 1774–1783 (2004).
9. Robock, A. Volcanic eruptions and climate. *Rev. Geophys.* **38**, 191–219 (2000).
10. Ayris, P. M. & Delmelle, P. The immediate environmental effects of tephra emission. *Bull. Volcanol.* **74**, 1905–1936 (2012).
11. Soreghan, G. S., Soreghan, M. J. & Heavens, N. G. Explosive volcanism as a key driver of the late Paleozoic ice age. *Geology* **47**, 600–604 (2019).
12. Lee, C.-T. A. et al. Volcanic ash as a driver of enhanced organic carbon burial in the Cretaceous. *Sci. Rep.* **8**, 4197 (2018).
13. Lee, C.-T. & Dee, S. Does volcanism cause warming or cooling? *Geology* **47**, 687–688 (2019).
14. Longman, J., Palmer, M. R., Gernon, T. M. & Manners, H. R. The role of tephra in enhancing organic carbon preservation in marine sediments. *Earth-Science Rev* **192**, 480–490 (2019).
15. Perron, M. M. G., Proemse, B. C., Strzelec, M., Gault-Ringold, M. & Bowie, A. R. Atmospheric inputs of volcanic iron around Heard and McDonald Islands, Southern ocean. *Environ. Sci. Atmos.* https://doi.org/10.1039/D1EA00054C (2021).
16. Jones, M. T. & Gislason, S. R. Rapid releases of metal salts and nutrients following the deposition of volcanic ash into aqueous environments. *Geochim. Cosmochim. Acta* **72**, 3661–3680 (2008).
17. Langmann, B., Zakšek, K., Hort, M. & Duggen, S. Volcanic ash as fertiliser for the surface ocean. *Atmos. Chem. Phys.* **10**, 3891–3899 (2010).
18. Achterberg, E. P. et al. Natural iron fertilization by the Eyjafjallajökull volcanic eruption. *Geophys. Res. Lett.* **40**, 921–926 (2013).
19. Olgun, N. et al. Surface ocean iron fertilization: the role of airborne volcanic ash from subduction zone and hot spot volcanoes and related iron fluxes into the Pacific Ocean. *Global Biogeochem. Cycles* **25**, n/a–n/a (2011).
20. Browning, T. J. et al. Strong responses of Southern Ocean phytoplankton communities to volcanic ash. *Geophys. Res. Lett.* **41**, 2851–2857 (2014).
21. Van Hulten, M. et al. Manganese in the west Atlantic Ocean in the context of the first global ocean circulation model of manganese. *Biogeosciences* **14**, 1123–1152 (2017).
22. Mahowald, N. M. et al. Aerosol trace metal leaching and impacts on marine microorganisms. *Nat. Commun.* **9**, 2614 (2018).
23. Tagliabue, A. et al. How well do global ocean biogeochemistry models simulate dissolved iron distributions? *Global Biogeochem. Cycles* **30**, 149–174 (2016).
24. Mahowald, N. M. et al. Atmospheric global dust cycle and iron inputs to the ocean. *Global Biogeochem. Cycles* **19**, https://doi.org/10.1029/2004GB002402 (2005).
25. Global Volcanism Program, T. *Volcanoes of the World, v4.8.4.* (Smithsonian Institution, 2013).
26. Chase, Z., Hales, B., Cowles, T., Schwartz, R. & van Geen, A. Distribution and variability of iron input to Oregon coastal waters during the upwelling season. *J. Geophys. Res. C Ocean.* **110**, 1–14 (2005).
27. Murray, N. A., McManus, J., Palmer, M. R., Haley, B. & Manners, H. Diagenesis in tephra-rich sediments from the Lesser Antilles Volcanic Arc: Pore fluid constraints. *Geochim. Cosmochim. Acta* **228**, 119–135 (2018).
28. Damby, D. E. et al. Assessment of the potential respiratory hazard of volcanic ash from future Icelandic eruptions: A study of archived basaltic to rhyolitic ash samples. *Environ. Heal. A Glob. Access Sci. Source* **16**, 98 (2017).
29. Oelkers, E. H. & Gislason, S. R. The mechanism, rates and consequences of basaltic glass dissolution: I. An experimental study of the dissolution rates of basaltic glass as a function of aqueous Al, Si and oxalic acid concentration at 25 °C and pH 3 and 11. *Geochim. Cosmochim* **65**, 3671–3681 (2001).
30. Wada, K. Minerals formed and mineral formation from volcanic ash by weathering. *Chem. Geol.* **60**, 17–28 (1987).
31. Rose, W. I. & Durant, A. J. Fine ash content of explosive eruptions. *J. Volcanol. Geotherm. Res.* **186**, 32–39 (2009).
32. Toggweiler, J. R., Dixon, K. & Broecker, W. S. The Peru upwelling and the ventilation of the south Pacific thermocline. *J. Geophys. Res.* **96**, 20467 (1991).
33. Calvo, E., Pelejero, C., Pena, L. D., Cacho, I. & Logan, G. A. Eastern Equatorial Pacific productivity and related-CO2 changes since the last glacial period. *Proc. Natl. Acad. Sci. U. S. A.* **108**, 5537–5541 (2011).
34. Sarmiento, J. L., Gruber, N., Brzezinski, M. A. & Dunne, J. P. High-latitude controls of thermocline nutrients and low latitude biological productivity. *Nature* **427**, 56–60 (2004).
35. Sawlan, J. J. & Murray, J. W. Trace metal remobilization in the interstitial waters of red clay and hemipelagic marine sediments. *Earth Planet. Sci. Lett.* **64**, 213–230 (1983).
36. Jones, M. T. et al. The weathering and element fluxes from active volcanoes to the oceans: A Montserrat case study. *Bull. Volcanol.* **73**, 207–222 (2011).
37. Raiswell, R. et al. Potentially bioavailable iron delivery by iceberg-hosted sediments and atmospheric dust to the polar oceans. *Biogeosciences* **13**, 3887–3900 (2016).
38. Poulton, S. W. & Raiswell, R. The low-temperature geochemical cycle of iron: From continental fluxes to marine sediment deposition. *Am. J. Sci.* **302**, 774–805 (2002).
39. Schroth, A. W., Crusius, J., Sholkovitz, E. R. & Bostick, B. C. Iron solubility driven by speciation in dust sources to the ocean. *Nat. Geosci.* **2**, 337–340 (2009).
40. Viers, J., Dupré, B. & Gaillardet, J. Chemical composition of suspended sediments in World Rivers: New insights from a new database. *Sci. Total Environ.* **407**, 853–868 (2009).
41. Paladio-Melasantos, M. L. et al. In *Fire and mud; eruptions and lahars of Mount Pinatubo, Philippines, Philippine Institute of Volcanology and Seismology, Quezon City* (eds. Newhall, C. G. & Punongbayan, R. S.) 413–535 (University of Washington Press, 1996).
42. Longman, J., Palmer, M. R. & Gernon, T. M. Viability of greenhouse gas removal via artificial addition of volcanic ash to the ocean. *Anthropocene* **32**, 100264 (2020).
43. Elrod, V. A., Berelson, W. M., Coale, K. H. & Johnson, K. S. The flux of iron from continental shelf sediments: A missing source for global budgets. *Geophys. Res. Lett.* **31**, n/a–n/a (2004).
44. Aller, R. C. In *Treatise on Geochemistry: Second Edition.* Vol. 8. 293–334 (Elsevier Inc., 2013).
45. Coale, K. H. et al. Southern ocean iron enrichment experiment: carbon cycling in high- and low-Si waters. *Science (80-.)* **304**, 408–414 (2004).
46. Jeandel, C. & Oelkers, E. H. The influence of terrigenous particulate material dissolution on ocean chemistry and global element cycles. *Chem. Geol.* **395**, 50–66 (2015).
47. Jeandel, C. Overview of the mechanisms that could explain the 'Boundary Exchange' at the land–ocean contact. *Philos. Trans. R. Soc. A Math. Phys. Eng. Sci* **374**, 20150287 (2016).
48. Lam, P. J. & Bishop, J. K. B. The continental margin is a key source of iron to the HNLC North Pacific Ocean. *Geophys. Res. Lett.* **35**, n/a–n/a (2008).
49. Nishioka, J. et al. Iron supply to the western subarctic Pacific: Importance of iron export from the Sea of Okhotsk. *J. Geophys. Res.* **112**, C10012 (2007).
50. Nishioka, J. et al. Intensive mixing along an island chain controls oceanic biogeochemical cycles. *Global Biogeochem. Cycles* **27**, 920–929 (2013).
51. Homoky, W. B. et al. Iron and manganese diagenesis in deep sea volcanogenic sediments and the origins of pore water colloids. *Geochim. Cosmochim. Acta* **75**, 5032–5048 (2011).
52. Homoky, W. B., John, S. G., Conway, T. M. & Mills, R. A. Distinct iron isotopic signatures and supply from marine sediment dissolution. *Nat. Commun.* **4**, 1–10 (2013).
53. Radic, A., Lacan, F. & Murray, J. W. Iron isotopes in the seawater of the equatorial Pacific Ocean: New constraints for the oceanic iron cycle. *Earth Planet. Sci. Lett.* **306**, 1–10 (2011).
54. Labatut, M. et al. Iron sources and dissolved-particulate interactions in the seawater of the Western Equatorial Pacific, iron isotope perspectives. *Global Biogeochem. Cycles* **28**, 1044–1065 (2014).

55. Abadie, C., Lacan, F., Radic, A., Pradoux, C. & Poitrasson, F. Iron isotopes reveal distinct dissolved iron sources and pathways in the intermediate versus deep Southern Ocean. *Proc. Natl. Acad. Sci. USA* **114**, 858–863 (2017).

56. Murray, N. A. et al. Data report: dissolved minor element compositions, sediment major and minor element concentrations, and reactive iron and manganese data from the Lesser Antilles volcanic arc region, IODP Expedition 340 Sites U1394, U1395, U1396, U1399, and U1400. *Proc. Integr. Ocean Drilling Program*, Vol. 340 (2016).

57. Brimhall, G. H. & Dietrich, W. E. Constitutive mass balance relations between chemical composition, volume, density, porosity, and strain in metasomatic hydrochemical systems: Results on weathering and pedogenesis. *Geochim. Cosmochim. Acta* **51**, 567–587 (1987).

58. Gernon, T. M., Hincks, T. K., Tyrrell, T., Rohling, E. J. & Palmer, M. R. Snowball Earth ocean chemistry driven by extensive ridge volcanism during Rodinia breakup. *Nat. Geosci.* **9**, 242–248 (2016).

59. Pyle, D. M. Mass and energy budgets of explosive volcanic eruptions. *Geophys. Res. Lett.* **22**, 563–566 (1995).

60. Gudmundsson, M. T. et al. Ash generation and distribution from the April-May 2010 eruption of Eyjafjallajökull, Iceland. *Sci. Rep.* **2**, 572 (2012).

61. Aiuppa, A. et al. Major-ion bulk deposition around an active volcano (Mt. Etna, Italy). *Bull. Volcanol.* **68**, 255–265 (2006).

62. Thorsteinsson, T., Jóhannsson, T., Stohl, A. & Kristiansen, N. I. High levels of particulate matter in Iceland due to direct ash emissions by the Eyjafjallajökull eruption and resuspension of deposited ash. *J. Geophys. Res. Solid Earth* **117**, 0–05 (2012).

63. Jutzeler, M. et al. On the fate of pumice rafts formed during the 2012 Havre submarine eruption. *Nat. Commun.* **5**, 1–10 (2014).

64. Rossi, E., Bagheri, G., Beckett, F. & Bonadonna, C. The fate of volcanic ash: premature or delayed sedimentation? *Nat. Commun. 2021 121* **12**, 1–9 (2021).

65. Jones, M. T. et al. Riverine particulate material dissolution as a significant flux of strontium to the oceans. *Earth Planet. Sci. Lett.* **355–356**, 51–59 (2012).

66. Wessel, P. & Smith, W. H. F. A global, self-consistent, hierarchical, high-resolution shoreline database. *J. Geophys. Res. B Solid Earth* **101**, 8741–8743 (1996).

Acknowledgements

Author contributions

J.L., M.R.P. and T.M.G. designed the study, interpreted the data and wrote the manuscript, with input from M.T.J. J.L. collated data and performed the modelling. H.R.M. performed ICP-MS analysis on sediment and ash samples and acquired the data. M.T.J. provided data from ash dissolution experiments and contributed to their interpretation.

Competing interests

The authors declare no competing interests.

Additional information

Supplementary information The online version contains supplementary material available at https://doi.org/10.1038/s43247-022-00389-7.

Correspondence and requests for materials should be addressed to Jack Longman.

Peer review information *Communications Earth & Environment* thanks the anonymous reviewers for their contribution to the peer review of this work. Primary handling editor: Clare Davis.

Reprints and permission information is available at http://www.nature.com/reprints

Publisher's note Springer Nature remains neutral with regard to jurisdictional claims in published maps and institutional affiliations.